Infacon XV: International Ferro-Alloys Congress, Edited by R.T. Jones, P. den Hoed, & M.W. Erwee,
Southern African Institute of Mining and Metallurgy, Cape Town, 25–28 February 2018

Chemical, microstructural, and phase changes of manganese ores in calcination and pre-reduction by natural gas

A. Cheraghi[1], H. Yoozbashizadeh[1], and J. Safarian[2]
[1]Sharif University of Technology (SUT), Azadi Avenue, N-1458889694, Tehran, Iran
[2]Norwegian University of Science and Technology (NTNU), Alfred Getz Vei 2, N-7491, Trondheim, Norway

Abstract – Using natural gas in the reduction of metal ores is sustainable as it is a cleaner energy source and reducing agent compared to solid carbonaceous materials such as coal and metallurgical coke. Natural gas is widely used in direct reduction of iron ore, which has shown significant growth in recent decades, and there is much interest in its usage for ferro-alloys production. In addition to sustainability, the application of natural gas has economic advantages in those geographical locations with large reserves. In the present study, the application of natural gas in the reduction of manganese ores is studied through experimental work. A Carbolite horizontal tube furnace was used to do complete calcination of commercial manganese ores at 900˚C in an inert atmosphere, followed by pre-reduction by natural gas at 1100˚C. Precise characterization of the ores, calcined ores, and reduced samples are carried out using X-Ray Diffraction, X-Ray Fluorescence, and Scanning Electron Microscopy techniques. It is shown that chemical, physical, and structural changes occur in the particles during calcination, with significant loss of mass. Methane shows a high reducing ability, and Mn species of the ores are reduced to lower oxygen-containing oxides, carbides, and even metallic phases. Oxide minerals show better reduction behaviour than silicates.

Keywords: manganese, ore, oxide, reduction, natural gas, calcination, ferromanganese

INTRODUCTION

Using a submerged arc furnace (SAF) is the prominent method in reduction of manganese (Mn) ores and in ferromanganese (FeMn) production. There are several disadvantages in using solid carbon sources as reducing agents, including environmental and financial issues. Studies show that the greatest amount of greenhouse gases in the whole FeMn production chain is due to carbon source consumption (Haque and Norgate, 2013). Several attempts have been made to perform solid-state reduction of the ores for both understanding the reaction mechanisms in the current commercial furnaces and developing gas-based technologies for solid-state reduction of the ore. Due to the low required oxygen partial pressure, reduction in solid state by graphite, hydrogen, or carbon monoxide does not go beyond MnO, and Mn metal/carbide is formed via carbothermic reduction of MnO from liquid slag (Safarian *et al.*, 2006). Literature studies show that using methane as reduction gas results in higher metallization and also faster reduction kinetics compared to the common carbothermic reduction processes (Bhalla and Eric, 2015). Moreover, it has been reported that the formation of carbide species is determined by the reduction temperature; Mn_7C_3 and Mn_5C_2 are formed at 1100°C and 1200°C respectively (Bhalla and Eric, 2015; Eric *et al.*, 2017). While no crack nor pore formation has been observed, the reduction has been reported to be limited to the ore surface (Eric *et al.*, 2017).

Using a mixture of methane and hydrogen for the reduction of pyrolusite shows that methane participates in carbide formation from MnO (Anacleto *et al.*, 2004b; Ostrovski and Zhang, 2006). The effect of iron oxide existence in the ore on Mn oxide reduction is controversial, and some have reported positive effects, due to faster reduction of iron oxide and taking the role of nuclei for Mn carbide formation (Akdogan and Eric, 1995). On the other hand, it is reported that iron oxide inhibits complete reduction, because of blockage of the porous plug by carbon produced from methane cracking on the reduced metallic iron surface (Anacleto *et al.*, 2004b; Ostrovski and Zhang, 2006). So, increasing the temperature to over 1150°C has been reported to be unfavourable, due to excessive methane cracking and carbon deposition (Anacleto *et al.*, 2004a; Ostrovski, 2014). In addition, formation of slag phases with a low melting point (at about 1150°C) has been reported to decrease the reduction rate, due to decreasing the reaction surface as a result of sintering (Anacleto *et al.*, 2004a; Ostrovski, 2014).

In the present study, the reduction of two commercial ores with different mineralogy (oxide and silicate Mn ores) by natural gas is studied. Calcination and pre-reduction behaviour of the ores is studied through XRD, XRF, and SEM-EDS characterization techniques, and more reducible compounds are identified.

EXPERIMENTAL PROCEDURE

Materials

Two different commercial Mn ores from two active mines in Iran were used as the raw materials: Venarch and Kerman ores. The former one is known as a silicate Mn ore and is considered as one of the most important Mn deposits in Iran and the Middle East. The ore samples were crushed, and a particle size range of 2.5–9.5 mm was chosen for all experiments. Argon and methane gases of 99.9% purity were also used as gaseous agents in the experiments.

Characterization

Quantitative chemical composition of the ores was studied by the X-Ray Fluorescence technique (Philips Magix-Pro XRF spectrometer (4 kV)). Phase analyses of ore samples, calcined samples, and pre-reduced samples were studied by the X-Ray Diffraction technique (Bruker D8 A25 DaVinci X-Ray Diffractometer with Cu-K_α radiation with a LynxEye™ SuperSpeed Detector). A 2θ range of 10–75 degrees was chosen as the diffraction angle, and a 0.2 degree step was chosen. For minimizing the risk of errors, the same powder as was used for XRF analysis was used for XRD experiments (smaller than 74 microns (200 mesh size)). The raw XRD data were processed by the commercial DIFFRAC.EVA software for phase analysis. For microstructural analysis, the samples were mounted by cold embedding epoxy resin Epofix (Struers). The varieties of colours and morphologies were considered to pick up representative particles from the samples. The polished samples were coated with a carbon layer and a high-resolution (1.2 nm) Hitachi SU-6600 field emission SEM. Qualitative and semi-quantitative chemical analysis was performed by Energy Dispersive X-Ray Spectroscopy (EDS) using a Hitachi Schottky-field emission electron source.

De-moisturizing

Sampling was accomplished by a quartering method. To ensure that weight changes in the calcination and reduction experiments were not the result of moisture removal, the samples were de-moisturized in the first step. Evaporating steel boats containing a mass of 800±1 g of the samples were dried in an oven overnight stay at 100°C in air.

Calcination and pre-reduction

Calcination and pre-reduction tests were carried out in a horizontal Carbolite tube furnace, illustrated schematically in Figure 1. In order to allow the gas to pass through the entire sample, a twisted stainless steel net with a mesh size of less than 1.5 mm was used as the sample container. The inside diameter of the tube was 37 mm and the stainless steel net was so twisted that it was fitted inside the tube. The container's length was as much as the hot zone of the furnace length (around 100 mm) and 80–100 g of the ore sample could be held in it.

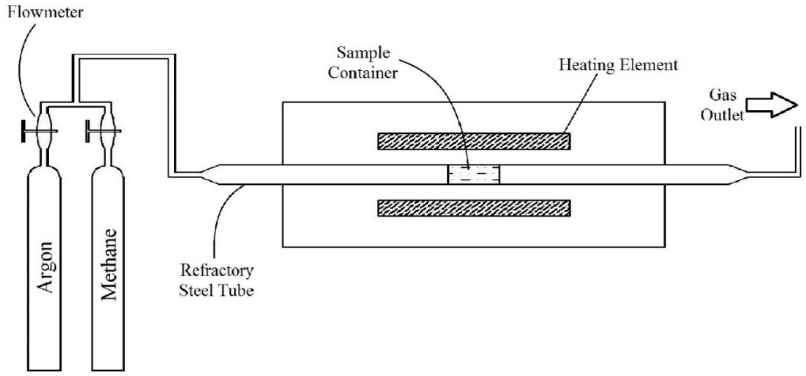

Figure 1: Schematic view of the tube furnace

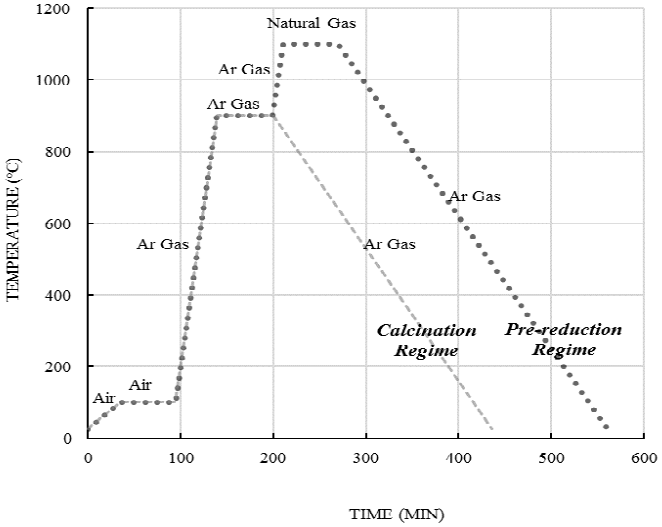

Figure 2: Heating and cooling profiles of calcination and pre-reduction tests

In order to provide a reliable temperature profile for the calcination and reduction trials, the thermocouple of the furnace was calibrated by checking the melting point of pure copper. The applied heating profile for calcination and reduction steps is shown in Figure 2. As can be seen, all calcination tests continued for 60 minutes at 900°C in an argon atmosphere. The argon gas flow rate was adjusted on 1 $L.min^{-1}$. For the pre-reduction step, the samples were first calcined, but, instead of cooling, they were heated up to 1100°C after calcination. After reaching 1100°C, the argon gas flow was reduced to half, and the reduction gas (CH_4) was introduced into the furnace. Isothermal reduction of the samples was carried out in a mixture of argon and methane (50% CH_4) with a gas flow rate of 1 $L.min^{-1}$. To ensure that the required amount of complete reduction was provided within the reduction period, the reduction was continued for 60 minutes. Thus, more than three times the required stoichiometric amount of methane for complete reduction was provided in the reduction step

(reaction [1]). The cooling and heating steps were carried out in an argon flow rate of 1 L.min^{-1} to avoid oxidation and re-oxidation.

$$7/17\ MnO_2 + CH_4\ (g) = 1/17\ Mn_7C_3 + 2\ H_2(g) + 14/17\ CO(g) \qquad [1]$$

RESULTS AND DISCUSSION

Characterization of the ores

Table I represents XRF quantitative analyses of the ore samples for the main elements. As observed, the Mn content is almost the same for both ore samples. Regarding relatively the same loss on ignition for the two ores, we may say that while the Kerman ore is richer in silica (about three times as much Si), Venarch ore has around 55% higher Fe and Ca concentrations than Kerman ore. Venarch ore also contains significantly higher concentrations of Na, Mg, and K.

Table I: Quantitative analysis of ore samples based on XRF analysis

Element	Na	Mg	Al	Si	P	S	K	Ca	Mn	Fe	Sr	As	Pb	Ba	L.O.I.
Venarch Ore	0.3	0.6	3.0	11.8	0.1	0.0	1.1	10.8	37.4	24.4	0.5	0.4	0.6	0.6	8.1
Kerman Ore	0.0	0.2	0.4	30.5	<0.1	<0.1	<0.1	7.0	35.0	15.5	<0.1	0.0	0.0	1.4	9.7

The XRD patterns of the two ores, and the characterized phases are shown in Figure 3. As the pattern shows, Venarch is a silicate ore, and Mn is present as braunite I (Mn_7SiO_{12}) in the ore. The pattern in some places matches other formats of braunite I that aluminium and calcium have substituted some Mn in the structure. As we do not see Al in other characterized phases, we may conclude that Al is completely associated with Mn in braunite I. The other phases in the Venarch ore are hematite (Fe_2O_3), quartz (SiO_2), and calcite ($CaCO_3$). Obviously, the main portion of Ca is in the free calcite phase, and the rest is in association with Mn, Si, and Fe oxides in different phases. It is worth noting that weak patterns of cryptomelane, strontium manganese silicate, and wollastonite were also observed in the phase analysis, and these phases may contain the observed (by XRF) K, Sr, and Na elements respectively.

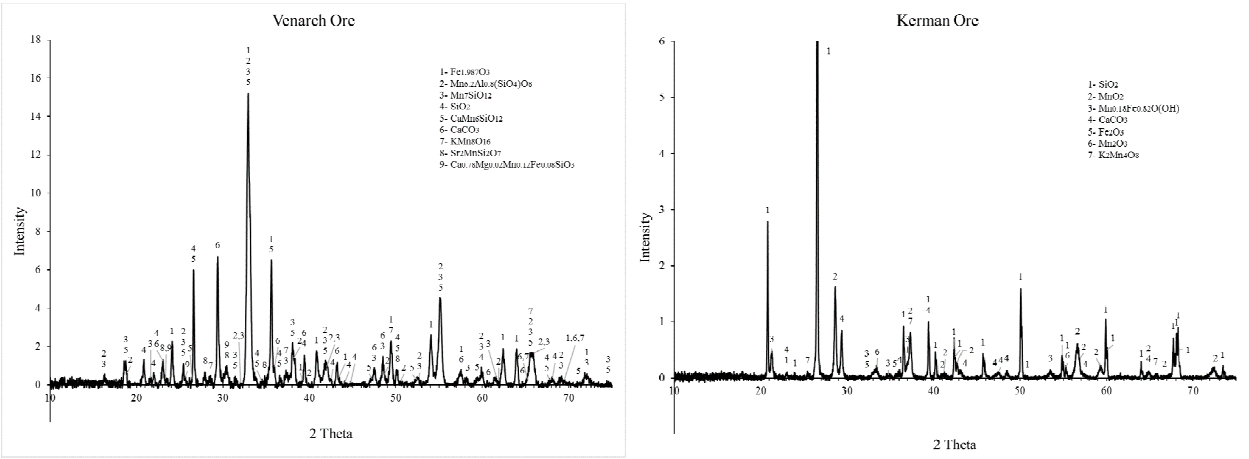

Figure 3: XRD patterns of Venarch and Kerman ores

The XRD analysis of Kerman ore (Figure 3) shows that Mn is present as pyrolusite (MnO_2) in Kerman ore. However, pyrolusite is not the prominent phase, as quartz appears in high intensity in the XRD spectrum. Obviously, the main portion of Mn exists as pyrolusite, and some as potassium manganese oxide ($K_2Mn_4O_8$). Weak patterns of Mn oxide in the form of Mn_2O_3 are also found in the XRD pattern. The

significant amount of Si (Table I) is in the form of free quartz phase, based on the XRD of Kerman ore (Figure 3). Iron is, however, in the free oxide form of hematite, and also in association with Mn in a (Fe,Mn)O(OH) phase. The significant amount of Ca in the ore (Table I) is obviously in the free calcite phase.

According to the information provided in Table I and Figure 3, the differences between the two ores are significant. Mn is present mostly as braunite with some elements in the structure and in silicate form in Venarch ore, while in Kerman ore it is less associated with other elements and mostly is in oxide form of pyrolusite. In addition, some Mn content of Kerman ore is engaged with iron in manganese-iron hydroxide. Although iron is present as hematite in both ores, the Venarch ore has a high amount of iron (Table I).

Ore behaviour in calcination

Experimental conditions and the mass changes in drying and calcination steps of the two samples are shown in Table II. Since the samples were de-moisturized before calcination, the reported weight changes in the Table are via dried samples. A comparison between L.O.I. (Table I) and the calcination weight changes of the samples (Table II) indicates a good correlation between XRF and large bath calcination data.

The XRD patterns of calcined samples and the characterized peaks are shown in Figure 4. The pattern shows that some calcination has occurred for Mn-containing species in the Venarch sample, as a bixbyite phase (Mn_2O_3) has been formed from braunite. However, there is still some un-decomposed braunite after calcination. Although there are still braunite and hematite phases in the structure, the intensities of the characteristic peaks are lower in the calcined sample, in comparison with the Venarch ore pattern in Figure 3. In addition, bixbyite and hedenbergite ($CaO.(Fe,Mn)O.2SiO_2$) peaks are also observed, indicating some calcination has occurred. On the other hand, calcite peaks are not observed in the calcined sample, while sharp CaO peaks are observed in the XRD pattern, showing complete decomposition of $CaCO_3$ to CaO.

Table II: Experimental details and weight changes in calcination and pre-reduction

No.	Ore	Process	Temp. (°C)	Gas	Duration (min)	Weight Change
1	Kerman	Drying	100	Air	60	-0.38%
2	Kerman	Calcination	900	Argon	60	-9.44%
3	Venarch	Drying	100	Air	60	-1.8%
4	Venarch	Calcination	900	Argon	60	-7.85%

The XRD pattern of the calcined Kerman sample is also shown in Figure 4. Thermal decomposition has occurred for the pyrolusite phase in the ore, and hausmannite (Mn_3O_4) has been formed. However, there is still a minor amount of pyrolusite in the structure. In addition, jacobsite ($(Mn,Fe)_3O_4$) phase has been formed in the sample. Calcium oxide (CaO) is another formed phase and no calcite peak is observed after calcination, indicating complete decomposition.

A different degree of thermal decomposition/calcination is observed in the two calcined samples. A comparison between the patterns of the two calcined samples reveals that, while hausmannite phase has been formed in the Kerman sample, there are bixbyite and un-decomposed braunite phases in the calcined Venarch sample. This could be due to less association of Mn with other elements in the Kerman sample. The

jacobsite phase in the calcined Kerman sample could be the result of calcination of manganese-iron hydroxide existing in the ore. No apparent phase change is observed for the hematite phase in the samples; however, the hematite peak intensity has decreased in the Venarch ore, due to the increase in the amount of the other phases after calcination.

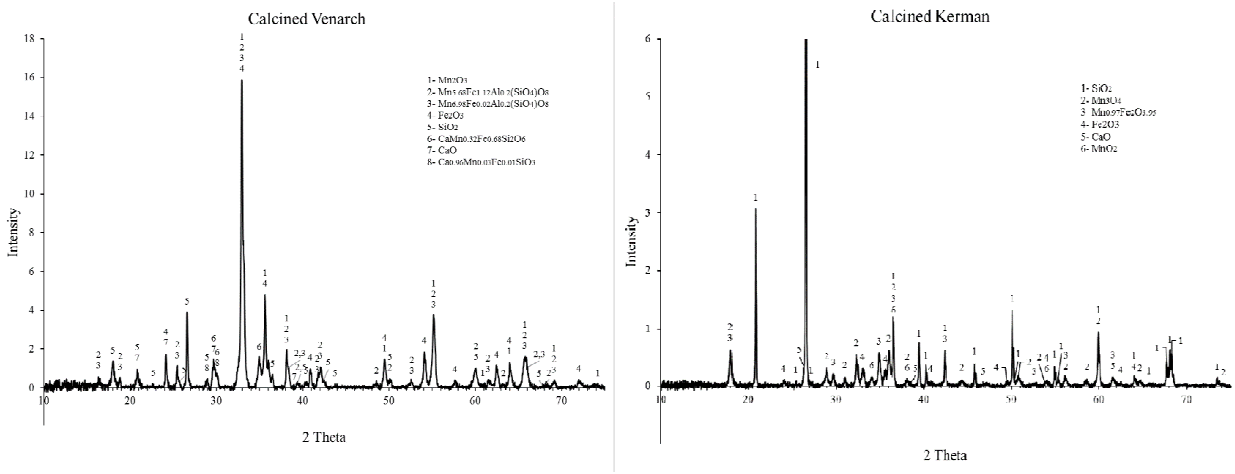

Figure 4: XRD patterns of calcined Venarch and Kerman samples in argon

Reduction by Natural Gas

In addition to XRD phase analysis, SEM-EDS analysis was done for the pre-reduced samples.

Figure 5: Pre-reduced Venarch sample at 1100°C in 50%CH_4–50%Ar for an hour

Pre-reduced Venarch sample

The pre-reduced sample was completely sintered and there were some partially melted particles on the net container, so the sample could be taken out only by crushing. Although the sample was mostly black, green particles could be seen in the sample and the sample had gained a greenish colour (Figure 5). Reduced samples were mainly covered, however, by a thin layer of soot. The surface of the particles had become spongy and small surface pores could be observed. Significant sintering between some particles was also observed.

The XRD pattern of the pre-reduced Venarch sample is shown in Figure 6. As the figure shows, MnO is the prominent phase, which is the reason for getting a greenish colour for the particles. This phase should have been produced from the braunite phase in the ore. Mn carbide phase is also observed in the XRD pattern. As seen, all

the hematite of the ore has been reduced to metallic iron and cementite (Fe_3C). As CaO and MnO show the XRD peaks at the same diffraction angle, it could not be stated with certainty that CaO is in high concentration amongst the phases, and further investigation is needed. In addition, CaO was not observed in EDS analysis of the selected sample particles and it can be a reason for low concentration of it. As calcite peaks have completely disappeared in the pattern, and CaO peaks were even observed in the calcined sample, CaO oxide is present in the pre-reduced sample, but at lower ranking order. This is more consistent with the XRF result of the ore (about 10 wt% calcium) and the fact that calcium is also present in three other phases of pre-reduced sample (Figure 6).

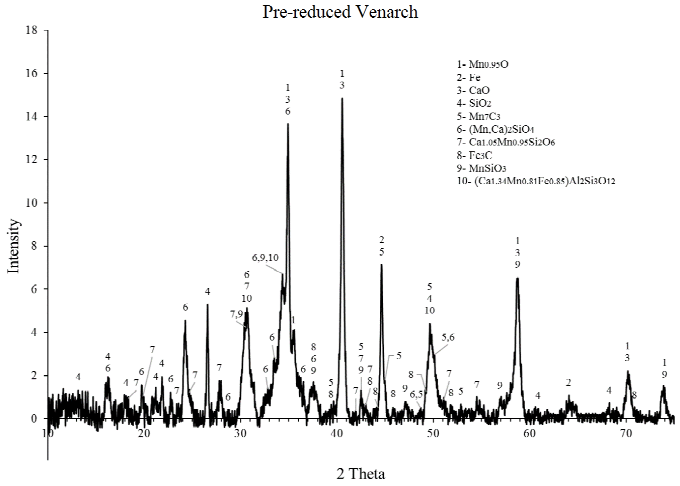

Figure 6: XRD pattern of pre-reduced Venarch sample

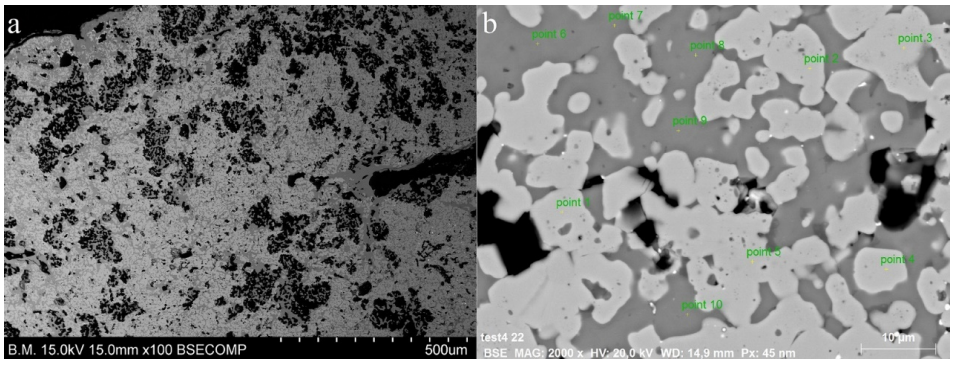

Figure 7: SEM-BSE image of greenish particles at magnifications of: a) 100× and b) 2000×

Different phases can be observed in SEM images in back-scattered electron (BSE) mode of one of the green particles in the pre-reduced sample, as shown in Figure 7. EDS multipoint analysis of the phases (Figure 7-b) shows that the bright phase (points 1 to 5) is MnO; while the dark phase (points 6 to 10) is characterized as tephroite with some calcium in the structure ($(Mn,Ca)_2SiO_4$), based on molar ratios. It could be concluded from the shape of the MnO phase in Figure 7-b that MnO grains have been nucleated and grown from the dominant braunite phase in the ore. Some particles have somewhat different chemical composition, and EDS multipoint analysis has shown (Mn,Fe)O with a high Mn/Fe ratio. As iron was mostly characterized as hematite in the ore sample, the (Mn,Fe)O phase could be formed as a result of solution of some FeO in MnO at elevated temperatures, which is favourable due to the small FeO activity in this solid solution. The rest of the hematite is reduced to metallic iron as described in the following.

EDS mapping of the shiny particles in the sintered area and the surrounding are shown in Figure 8. As the figure shows, the shiny particles are rich in iron, and the dendritic phase has a higher Mn concentration than the dark matrix phase. High iron concentration in shiny particles is also confirmed by EDS point analysis. This metallic iron has been produced directly from hematite. As the EDS mapping shows, the dendritic phase has a higher Mn concentration and is schefferite ($(Ca,Mn)(Mg,Fe,Mn)Si_2O_6$). EDS point analysis indicates that the dark matrix phase is bustamite ($CaMnSi_2O_6$). However, some minor differences over different particles is also observed in EDS multipoint analysis; in some other particles, schefferite dendrites have been observed in the grossular ($(Ca,Mn,Fe)_2Al_2Si_3O_{12}$) matrix phase. This difference is raised from the difference in the ore phases and different formats of braunite that were characterized in the ore sample. In other words, heterogeneity of the ore has resulted in heterogeneity in the pre-reduced sample as well. In addition to the metallic phase, carbides of Mn and Fe were found and characterized by EDS analysis, confirming the observation of carbides in the XRD spectrum in Figure 6. It is worth mentioning that significant smelting and sintering is observed in the microstructural analysis of the pre-reduced sample in many locations of the reduced bed. The shape of the phases in the SEM image may clearly show this phenomenon. As the process temperature is 1100˚C, the melting/sintering of phases may be attributed to the extensive exothermic reduction reactions of the Mn oxides, which cause a temperature rise to higher temperatures in the sample. In addition, and based on three-phase diagrams, the silicate ores reveal a lower melting point than oxide ores (Anacleto *et al.*, 2004a).

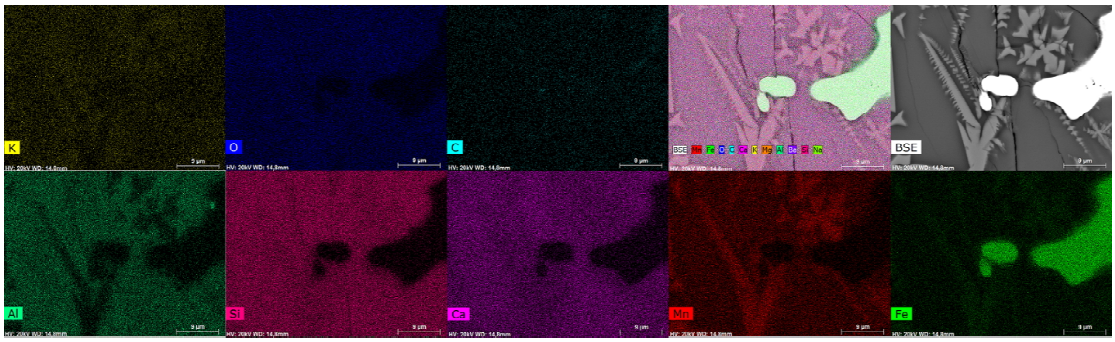

Figure 8: EDS mapping of shiny particles in sintered area at magnification of 2000

Pre-reduced Kerman sample

Unlike the Venarch sample, no sintering could be observed in the pre-reduced Kerman sample. In addition, the sample had been brittle and full of cracks. The entire sample was completely covered by soot and had a dark colour. Moreover, some metallic-like shiny particles were observed on the pre-reduced particles.

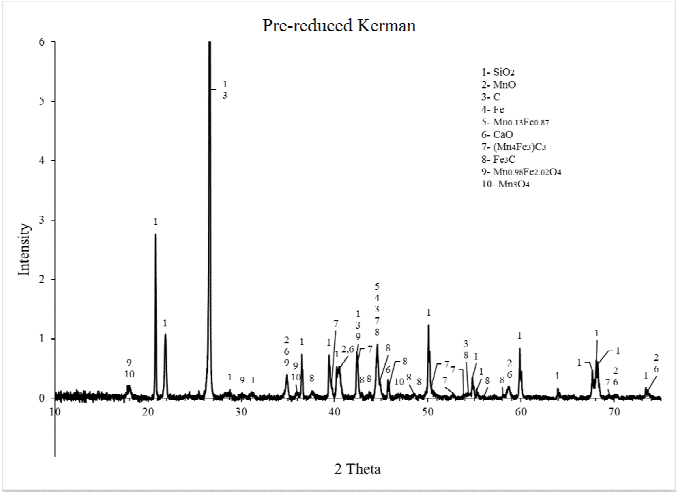

Figure 9: XRD pattern of pre-reduced Kerman sample

Figure 9 shows the XRD pattern of the pre-reduced Kerman sample. As expected, SiO_2 is the prominent phase and no apparent change has occurred to this phase. Obviously, the other prominent phase is MnO that is formed from the pyrolusite phase of the raw ore. The XRD pattern shows that, in addition to the mixed carbide of Mn and Fe, a metallic FeMn phase has also formed. This indicates that the pre-reduction has significantly occurred by methane. As there are not many phases including both iron and Mn in the ore (only manganese iron hydroxide) and in the pre-reduced sample, we may conclude that metallic iron and Mn have been dissolved in each other, forming the FeMn phase, which is thermodynamically favourable. As the XRD pattern shows, there is some carbon in the sample, which is the reason for the dark colour of the sample.

EDS mapping of the pre-reduced Kerman particles are shown in Figure 10. Many cracks have been formed, which are seen as the area rich in carbon. Two main areas are observed in the EDS mapping image; one rich in Mn, and one rich in silicon, which are MnO and SiO_2 respectively. Although some metallic FeMn is observed in the mapping image (mostly surrounded by the MnO phase), the high carbon concentration in resin makes it impossible to detect this phase properly. In fact, this phase could be a FeMn carbide phase. Moreover, carbide phase presence is approved by the XRD pattern (Figure 9). The porous phase should have been pyrolusite, as the metal/carbide phases are formed mostly near the pores that had been in contact with CH_4 gas. There is some rhodonite ($MnSiO_3$) within quartz phase that should have been the reduced tephroite phase ($MnSiO_4$) in the raw ore.

Some narrow veins of calcite were observed in a SiO_2 matrix, and some CaO phase had been formed between calcite and silicon oxide. In addition to the pre-reduced Kerman XRD pattern (Figure 9), CaO peaks were observed in the calcined Kerman XRD pattern (Figure 4). Although CaO and MnO show the XRD characteristic peaks at the same diffraction angle, there was no MnO in the calcined sample. This shows that most of the calcite should have been calcined, but some of it remained.

Metallic iron is distributed all over the sample (both inside and near the surface), due to the formation of many cracks and proper penetration of gas into the particles. A slight Mn concentration in metallic iron was observed in some areas. This shows that this phase has been either manganese iron hydroxide or hematite in the ore sample (Figure 3). In the latter case, some Mn has been dissolved in the hematite phase. It is

worth mentioning that rhodonite ($MnSiO_3$) and wollastonite ($(Mn,Ca)SiO_3$) were also observed in the reduced sample by EDS multipoint analysis and their molar ratios.

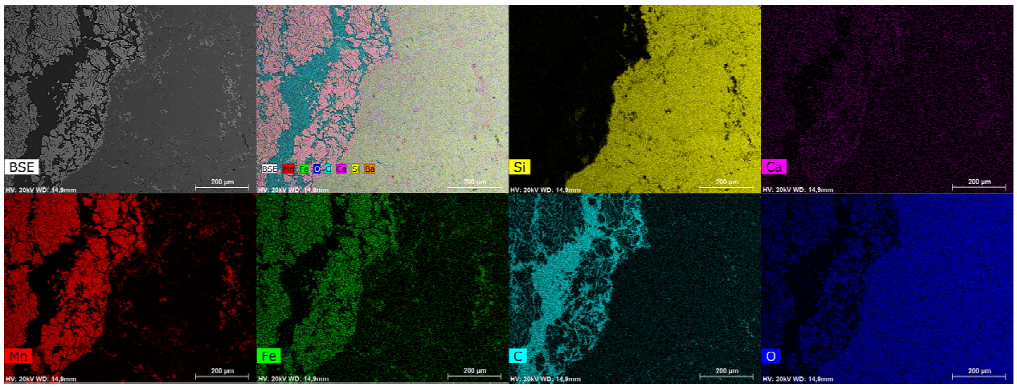

Figure 10: EDS mapping of round particles in pre-reduced Kerman sample at magnification of 100X

CONCLUSIONS

The calcination and CH_4 reduction of Mn ores were done through experimental work, and the behaviour of original phases in the ores in calcination and reduction were studied. The main conclusions are:

- A combination of XRF, XRD, and SEM-supported by EDS is very useful in recognising the phases in the ore samples, and high-temperature treated samples. The combination of these techniques provides a proper overview of the phases, especially in species showing characteristic peaks at the same diffraction angle, such as MnO and CaO in XRD.
- Hausmannite is formed from pyrolusite in calcination of oxide ore (Kerman), while bixbyite is formed from braunite in calcination of silicate ore (Venarch); a more convenient behaviour of pyrolusite thermal decomposition.
- While hematite is rarely reduced in calcination, complete reduction to metallic iron was observed in reduction by CH_4. Remaining iron oxide and co-existing MnO produced in reduction tend to dissolve in each other at high temperatures, forming FeO-MnO solutions.
- Although MnO is the main Mn-containing phase in both pre-reduced samples, metallic iron, Mn carbides, and Fe-Mn particles are obtained through reduction by CH_4. More FeMn was produced in the oxide ore, which was detectable by XRD analysis.

ACKNOWLEDGEMENTS

This study has been done in the laboratories at SUT and NTNU, and the support from both universities is acknowledged. This work has also been supported by the Research Domain 2 in SFI-Metal production – a Norwegian Centre for Research-Based Innovation.

REFERENCES

Akdogan G. and Eric R.H. 1995. Kinetics of the solid-state carbothermic reduction of Wessel manganese ores, *Metallurgical and Materials Transactions B,* 26(1), pp.13–24.

Anacleto N., Ostrovski O., and Ganguly S. 2004a. Reduction of manganese ores by methane-containing gas, *ISIJ international,* 44(10), pp.1615–1622.

Anacleto N., Ostrovski O., and Ganguly S. 2004b. Reduction of manganese oxides by methane-containing gas, *ISIJ international,* 44(9), pp.1480–1487.

Bhalla A. and Eric R.H. 2015. Reduction behavior of manganese ore using methane gas, *Infacon XIV: The Fourteenth International Ferroalloys Congress*, Kyiv, Ukraine, 31 May – 4 June 2015, pp.461–469.

Eric R.H., Bhalla A., Halli P., and Taskinen P. 2017. Solid state reduction of iron, manganese and chromium oxide ores with methane, *Applications of Process Engineering Principles in Materials Processing, Energy and Environmental Technologies*: Springer, pp.307–318.

Haque N. and Norgate T. 2013. Estimation of greenhouse gas emissions from ferroalloy production using life cycle assessment with particular reference to Australia, *Journal of cleaner production,* 39, pp.220–230.

Ostrovski O. 2014. The use of natural gas for reduction of metal oxides: Constraints and prospects, *Celebrating the Megascale*: TMS, Springer, pp.529–536.

Ostrovski O. and Zhang G. 2006. Reduction and carburization of metal oxides by methane-containing gas, *AIChE Journal,* 52(1), pp.300–310.

Safarian J., Grong Ø., Kolbeinsen L., and Olsen S.E. 2006. A process model for the carbothermic reduction of MnO from high carbon ferromanganese slag—The model, *ISIJ International,* 46(8), pp.1120–1129.

Alireza Cheraghi

PhD Candidate, SUT & NTNU

Bachelor and Master degrees in Materials Science and Engineering at Sharif University of Technology (SUT), Tehran, Iran. Currently, PhD candidate at SUT and exchange PhD at NTNU. PhD thesis title: Pre-reduction of Manganese Ores by Natural Gas.